THE DEVELOPMENT OF A PASSIVE ACOUSTIC DEVICE FOR MONITORING THE EFFECTIVENESS OF SHOCKWAVE LITHOTRIPSY IN REAL TIME

TIMOTHY LEIGHTON[1], FIAMMETTA FEDELE[2], ANDREW COLEMAN[2], CATHERINE MCCARTHY[2], AHMAD JAMALUDDIN[3], CARY TURANGAN[3], GRAHAM BALL[4], SIMON RYVES[5], ANDREW HURRELL[6], ANTONELLO DE STEFANO[7], PAUL WHITE[1]

[1] Institute of Sound and Vibration Research, University of Southampton,
Highfield, Southampton SO17 1BJ, UK
tgl@soton.ac.uk

[2] Medical Physics Department, Guy's and St Thomas' NHS Foundation Trust,
Lambeth Palace Road, London SE1 7EH, UK

[3] School of Engineering Sciences, University of Southampton,
Highfield, Southampton SO17 1BJ, UK

[4] Atomic Weapons Establishment,
Aldermaston, Reading, RG7 4PR, UK

[5] Stone Unit, Day Surgery Department, Guy's and St Thomas' NHS Foundation Trust,
St Thomas Street, London SE1 9RT, UK

[6] Precision Acoustics Ltd., Hampton Farm Business Park,
Higher Bockhampton, Dorchester DT2 8QH, Dorset, UK

[7] Radiological Science Group**,** Medical Physics Department, St Mary's Hospital,
Portsmouth PO3 6AD, Hampshire, UK

This paper reports how laboratory experiments and hydrocode simulations (of cavitation and shock wave propagation) have been used to generate a clinical device which can deliver real benefit to patients with kidney stones. Currently X-ray or ultrasound B-scan imaging are used to locate the stone and to check that it remains targeted at the focus of the lithotripter during treatment. Neither imaging method is particularly effective in allowing the efficacy of treatment to be judged during the treatment session. In this study, laboratory experiment and Computational Fluid Dynamics simulations of the complex interactions between the shock wave, the stone, and the human tissue, have been used to develop a new clinical device. This device, which has been tested in clinical trials, exploits the passive acoustic emissions generated by these interactions, to identify whether the stone remains in the focus, and to what extent the treatment has been successful.

INTRODUCTION

Extracorporeal shock wave lithotripsy (ESWL) was introduced in the 1980s and has become the preferred modality for the non-invasive treatment of renal and ureteric stone disease. The treatment involves focusing several thousand acoustic shock waves on the stone to generate stone fragments that are small enough to be passed naturally from the body, or more effectively dissolved by drugs [1]. Currently, around 30% to 50% of patients need re-treatment with ESWL [2], with some of these patients undergoing more than three treatments for the same stone [3-5]. Re-treatment is a useful option, but involves additional morbidity due, amongst other things, to the bruising of tissue caused by the passage of the shock wave [6].

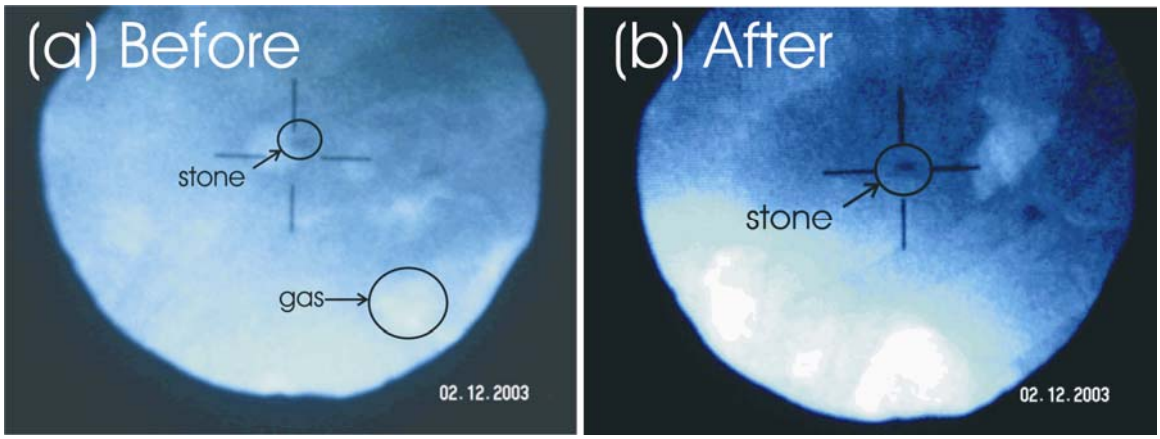

Fig.1 X-ray image of a stone (a) before and (b) immediately after ESWL

This paper reports on a seventeen-year activity, begun by Leighton and Coleman in the early 1990s, to develop the first clinically-proven passive acoustic device to offer the opportunity of reducing retreatment rates by addressing two factors which are key to reducing the likelihood of retreatment[†] [7]. These factors are:

[†] Note, however, that the ethical permissions under which the clinical trials were performed specifically excluded our providing the clinicians with information which would alter the treatment. Therefore our clinical studies could not specifically test retreatment rates. This UK team is unlikely to be able to secure funding to undertake such follow-up trials.

- maintenance of good targeting - if the focus of the shock wave moves of the stone, and onto healthy tissue, not only is the likelihood of fragmenting the stone reduced, but healthy tissue may receive unwanted shock exposure;
- real-time monitoring of whether each shock contributed significantly to stone fragmentation – the detection of a series of ineffective shocks would indicate to the clinician that the treatment parameters may need further examination (e.g. retargeting may be in order);
- an indication of the cumulative effectiveness of the shocks given to date in a single treatment (which for example could indicate whether it is appropriate to terminate the treatment).

The device generated in this study provides an indicator of all three features (the second two are referred to as $TS(t)$ and TS_0 respectively in this study). This feedback is important because, although a range of physical factors probably influences the stone-free rate and morbidity associated with ESWL treatment (including the stone size, location and density, the anatomical position and the body mass index of the patient [4,8,9]), the output of the Passive Acoustic Sensor (PAS) developed in this study provides information which is directly relevant to changes that can be made by the lithotripter operator during treatment to enhance the procedure. The maintenance of accurate targeting throughout the treatment, for example, is under operator control using ultrasound or X-ray imaging systems (Figure 1(a)) and can be expected strongly to influence treatment effectiveness [10]. Whilst X-ray or ultrasound B-scan imaging are used to locate the stone and to check that it remains targeted at the focus of the lithotripter during treatment, neither imaging method is particularly effective in allowing the efficacy of treatment to be judged during the treatment session.

The operator also selects the shock wave strength setting, typically using the highest setting compatible with the level of pain tolerated by the patient [3]. Ideally the operator would also have a role in limiting the morbidity associated with shock wave exposure [12], for example by terminating the treatment when the stone has fully fragmented. In practice, the current imaging systems are largely inadequate for indicating when stone fragmentation is complete [13]; Figure 1(b)) and the strategy almost universally adopted by ESWL operators is to deliver a pre-defined number of shock waves (typically around 3000). Finally, the operator has a significant role in minimising the ionising radiation exposure by restricting the fluoroscopy exposure time and number of spot films, within the constraint of achieving accurate shock wave targeting of the stone [14]. More information on treatment progress and targeting during clinical ESWL may allow the operator to exercise greater control over many of the factors that influence re-treatment rate and morbidity.

This article describes a new passive device that provides the ESWL operator with information on the maintenance of accurate targeting of the stone and a measure of the effectiveness of the treatment. The device consists of a passive acoustic sensor placed on the patient during treatment that monitors the acoustic signal scattered when the shock wave impinges on the stone and surrounding tissues. This signal is processed in real-time to provide easily interpreted visual cues to the ESWL operator. These cues can be used to inform decisions related to the need for re-targeting and to the ongoing effectiveness of the treatment. This paper reports on a clinical study, in which the performance of the device has been compared with measures of the degree of stone fragmentation obtained from pre- and post-ESWL X-ray films

interpreted by clinical staff immediately after treatment, and at the follow-up appointment three weeks later.

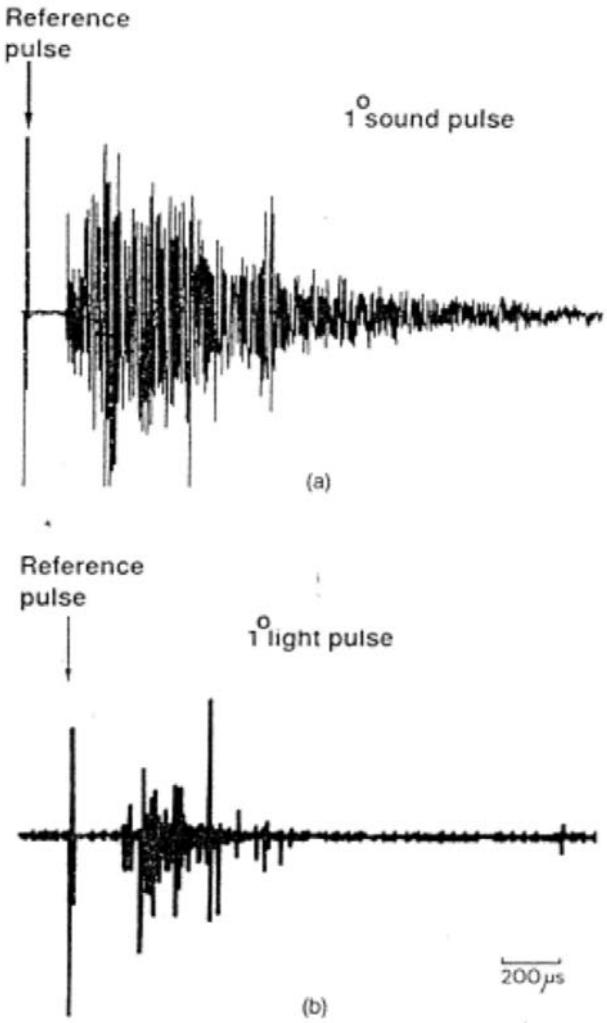

Fig.2 (a) The acoustic emission detected with an early form of the passive acoustic detector (shown in Figure 3). (b) The photomultiplier record of the sonoluminescence from a similar discharge by the same lithotripter (the two records could not be acquired simultaneously in this early experiment). From Coleman *et al.* [11]

The development of the clinical system described in this paper has previously proceeded through a series of studies, specifically:

- Stage 1 (detailed in Section 1): This stage combined modelling with laboratory experimentation to determine the key passive acoustic signature that would be used [11, 15, 16];
- Stage 2 (detailed in Section 2, and conducted in parallel with Stage 3): This stage used computational fluid dynamics (CFD) studies of single bubbles to clarify the interaction between shock wave, bubble, stone and tissue [17, 18]. These CFD studies were then expanded to include the interaction of multiple bubbles with each

other, and with the shock, tissue and stone; it was also used to predict what pressure signature would be detected in the far field from the pressure fields predicted by the CFD in the proximity of the stone;

- Stage 3 (detailed in Section 3, and conducted in parallel with Stage 2): informed by the ongoing CFD results, laboratory experiments were conducted using a series of prototype passive acoustic detectors, to determine the properties of the acoustic signal and how it changes with the accuracy of the targeting and the degree of stone fragmentation [19-24];
- Stage 4 (detailed in Section 4): Preliminary *in vivo* studies were undertaken to develop the sensor, the control and analysis software, and the procedures, for use in theatre [7, 24];
- Stage 5 (detailed in section 5): Two clinical trials were undertaken. For the first trial, the results of Stages 3, 4 and 5 were combined to determine a postulated *a piori* set of 'rules' against which the passive acoustic signal could be characterized to judge whether it had been successful in assessing targeting and stone fragmentation (using the sensors designed in Stage 4). In the first clinical trial, these 'rules were then tested against a set of patients in the clinic. The performance of the equipment was also tested. Analysis of the results of the first clinical trial allowed: (*i*) adaptations to be made to the hardware to make it more robust; (*ii*) the 'rules' used to judge the effectiveness of the shocks to be adapted to account for the differences between the *in vitro* and *in vivo* scenarios; and (*iii*) generation of the in-theatre *SEAC* (Secondary Emissions Analysis in Clinic) software for control and data acquisition of the device to be developed to final form. In the second clinical trial, these three innovations were tested against the outcome of treatment, and the performance for the PAS was assessed [7, 24].

These stages will now be described.

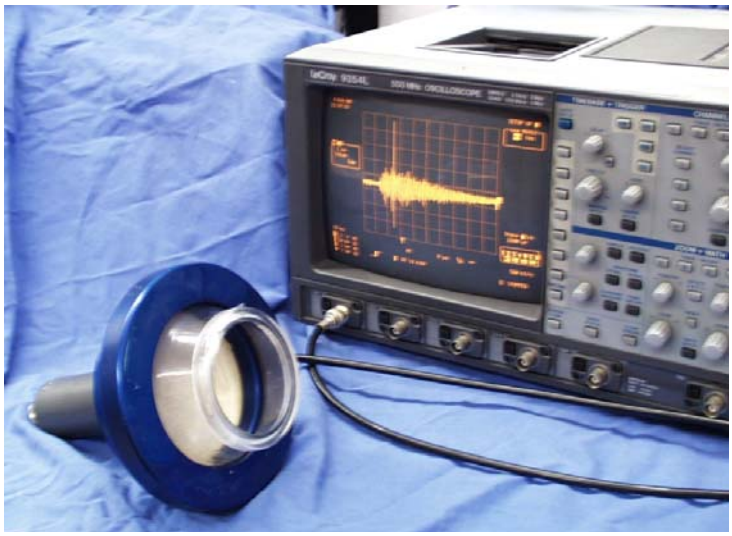

Fig.3 This early form of the sensor for passive acoustic emissions was based upon a focused bowl hydrophone having a natural frequency of 1 MHz. The output from the device is displayed on the oscilloscope, showing the characteristic two-peak structure

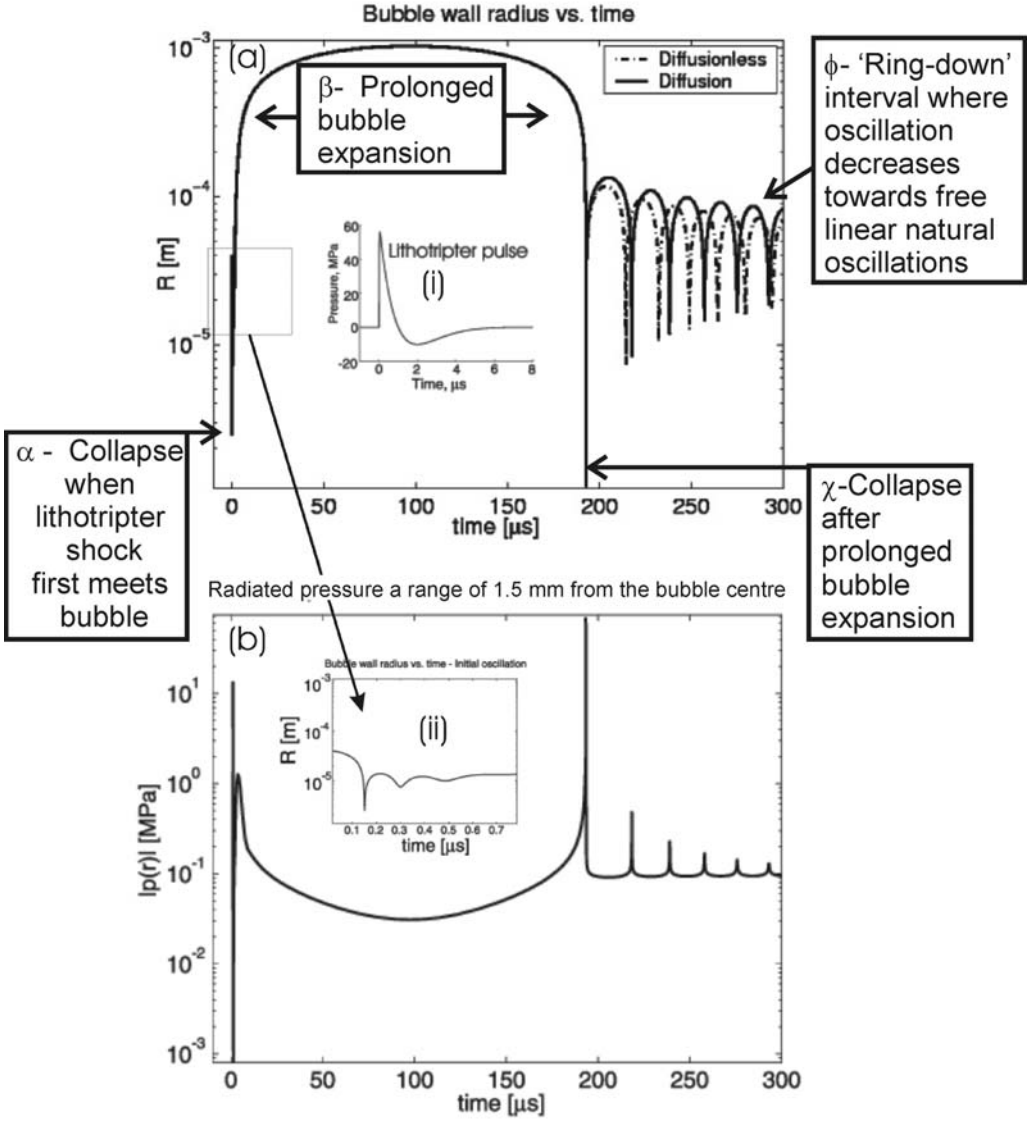

Fig.4 An air bubble of initial radius 40 microns in water is subjected in the free field to the lithotripter pulse shown in inset (i) (Peak positive pressure = 56 MPa; Peak negative pressure = -10 MPa). (a) The bubble radius against time is shown, as predicted by the Gilmore model, with (solid line) and without (dashed line) mass flux across the bubble wall. Note that the inclusion of diffusion makes the final bubble size greater than the initial size, with a consequent slight decrease in the period of the oscillations (i.e. a reduction in the frequency) at the timescales marked χ. Inset (ii) shows the micro-rebounds that are visible in the fine detail of the collapse which occurs around t=0. Similar features are seen in the CFD predictions (Turangan *et al.* [18]). (b) On a common time axis with (a) and for the same bubble collapse, the pressure that would be measured 1.5 mm away from the bubble centre is shown. Two main emissions (at $t \approx 0$ μs and at $t \approx 190$ μs) are associated with rebounds in (a), subsequent emissions being smaller. The overall effect of such pairs of emissions from the collapse of a cloud of bubbles was identified as demarcating the interval t_c in the early 1990s [11, 15, 16]. The labels in square boxes are explained in the text

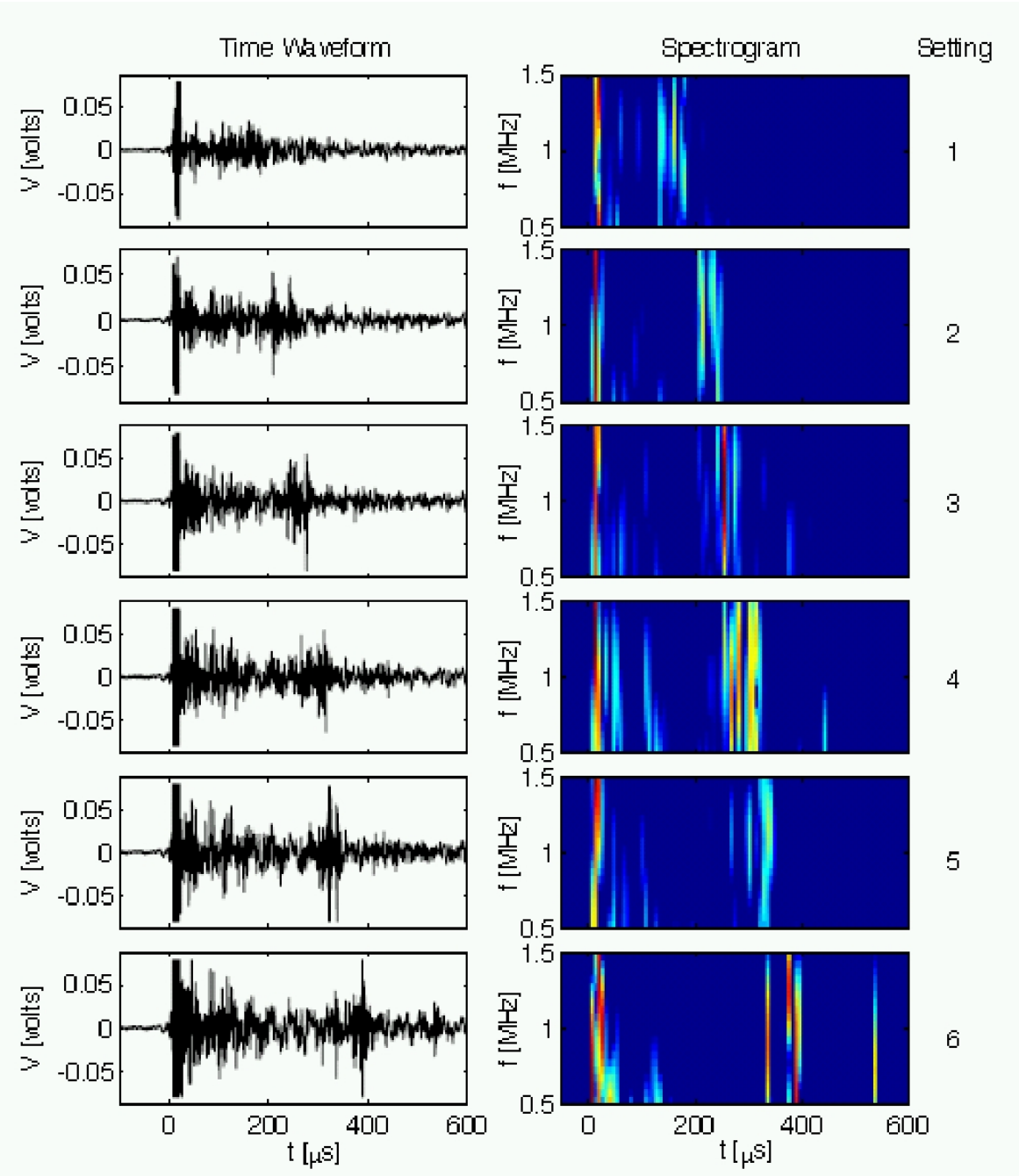

Fig.5 Data from a single patient, with the lithotripter setting increasing down the page from 1 to 6 (as shown on the far right), showing on the left the time history of passive acoustic emissions detected with the early version of the sensor shown in Figure 3. To the right of each time history is the corresponding spectrogram of the signal. Transient broadband signals are generated by cavitation. If one requires (as did the authors for modeling) some 'typical' bubble size which might persist from one lithotripter pulse to the next, then an estimate from this could be obtained from the emissions detected at the greater times. Taken from Cunningham *et al.* [25]

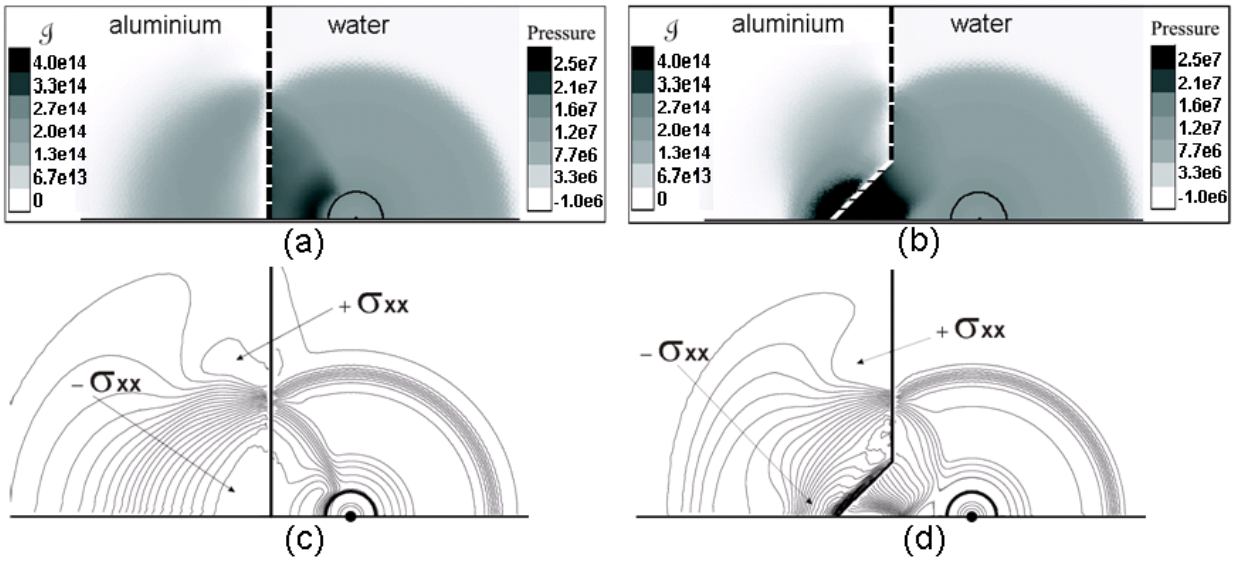

Fig.6 Axi-symmetric plots of the distributions of pressure and stress, are indicated for the expansion of a bubble near planar and notched aluminium walls, after a high speed jet has passed through the bubble (a situation which can only be modelled with any accuracy by a simulation which includes liquid compressibility). Whilst not an exact match (see below), in the context of this paper this scenario resembles the situation approximately at the time associated with the generation of the signal m_2. The location occupied by the bubble wall (when it was stationary with an internal pressure greater than that in the surrounding liquid) is indicated by the semicircle. The axis of symmetry is at the base of each frame. The bubble is close to solid aluminium which is planar (a,c) or notched (b,d). Air/water and water/aluminium interfaces are shown by dashed (a,b) or thick black (c,d) lines, with a horizontal axis of rotational symmetry at the base of each frame. In the greyscale images (a,b), the right half of each plot refers to the pressure in the water (given in Pa), but on the left of each plot (in the aluminium) the greyscale plots the second invariant of stress [$\mathcal{J}$, units Pa^2]. For this aluminium model with 0.3G Pa yield strength, elastic-plastic yield will occur in aluminium when the value of $\mathcal{J}$ exceeds 6×10^{16} Pa^2. Although the aluminium is still under elastic phase, the notch introduces stress concentration and a greater likelihood[7] of failure (c.f. fig. 5.57 of reference [16]). Parts (c,d) show the total stress σ_{xx} contours in aluminium parallel to the rotational axis, and pressure contours in water and bubble, for 1 MPa contour intervals ($-\sigma_{xx}$ in aluminium indicates compression, and $+\sigma_{xx}$ indicates tension). For details see reference [18]

1. INCEPTION OF THE IDEA THROUGH MODELLING AND EXPERIMENTATION

In 1990 Leighton and Coleman correlated the typical two-peak passive acoustic emission observed when lithotripsy occurred in a test tank (Figure 2(a)), with the temporal profile of sonoluminescent emissions which were indicative of cavitation (Figure 2(b)). They used the passive acoustic sensor shown in Figure 3. They suggested that the source of the first peak was the cavitational collapse which results when the lithotripter first meets the bubble (Figure 4, label α). After this collapse, the Gilmore model suggests that the bubble undertakes a prolonged expansion phase (Figure 4, label β), before collapsing again (at which time the second peak in acoustic emission and luminescence is generated; see Figure 4, label χ). These studies are

described in references [11, 15, 16]. The bubble must remain spherical and intact in the Gilmore model, so that after this second collapse the bubble oscillates with gradually decreasing amplitude, with a frequency which tends ever more closely to its 'Minnaert' frequency as time proceeds (Figure 4, label ϕ). Of course the real cavitational bubble will undergo a host of other behaviours that are not included in the Gilmore model, including:

- departures from sphericity;
- bubbles fragmentation and coalescence;
- interaction with other bodies (other bubbles, stones etc.) in the liquid;
- the presence of pressure fields and flows which are not spherically symmetric with respect to the bubble centre, and which may change over lengthscales which are not very much greater than the bubble radius.

However the Gilmore model has proved to be an extremely useful tool (in part through phenomenon which bring the overall behaviour of a cloud of bubbles into closer alignment with its rather limiting assumptions, an example being when fragmentation during a collapse can be reversed through coalescence of the fragments during the subsequent expansion phase [26-28].

Therefore Leighton and Coleman conceived of developing a passive acoustic sensor to monitor targeting and fragmentation in real time in the clinical during lithotripsy. This required a sequence of research tools to be developed, and a series of knowledge gaps to be filled. An example of a research tool is the CFD approach described in Section 2, which overcame the assumptions listed by bullet-point above. An example of the knowledge gap is in the form of an appropriate value for the initial bubble size R_0 to use in the CFD simulations and the Gilmore modeling of the form shown in Figure 4. A useful value of $R_0 \approx 40\mu$m was arrived at by applying the $\alpha,\beta,\chi,\varphi$ interpretation described above to *in vivo* records [25] (Figure 5)).

2. COMPUTATIONAL FLUID DYNAMICS STUDIES

As stated in Section 1, CFD studies were implemented to provide a method of simulating the interaction of bubbles, tissues and stones without the limitations of assuming that the spatial scales of the pressure perturbations are long with respect to the bubble radius, and without the assumption of spherical symmetry in the bubble and the liquid, and free field conditions [17, 30-33]. The free-Lagrange technique used is described in detail in Turangan *et al.* [18]. As an example, Figure 6 illustrates how techniques were developed to incorporate the presence of solids close to the bubble, and methods by which those boundaries may incorporate cracks and notches. In these simulations, real material properties can be assigned to the solid. Maps of the evolution of an index reflecting the likelihood of failure (Figure 6(a,b)) can be made from the stresses calculated within it (Figure 6(c,d)). The method has been extended to estimate the emission from a population of O(1000) bubbles distributed throughout the focus of the lithotripter (Figure 7). Whilst the first simulations of the pressures close to single bubbles are found in references [17, 18, 30-33], details of the techniques used to generate the far field pressures from the pressure field predicted close to the bubble by the CFD simulations, and the simulation of the effects of multiple bubbles, will be detailed in future papers.

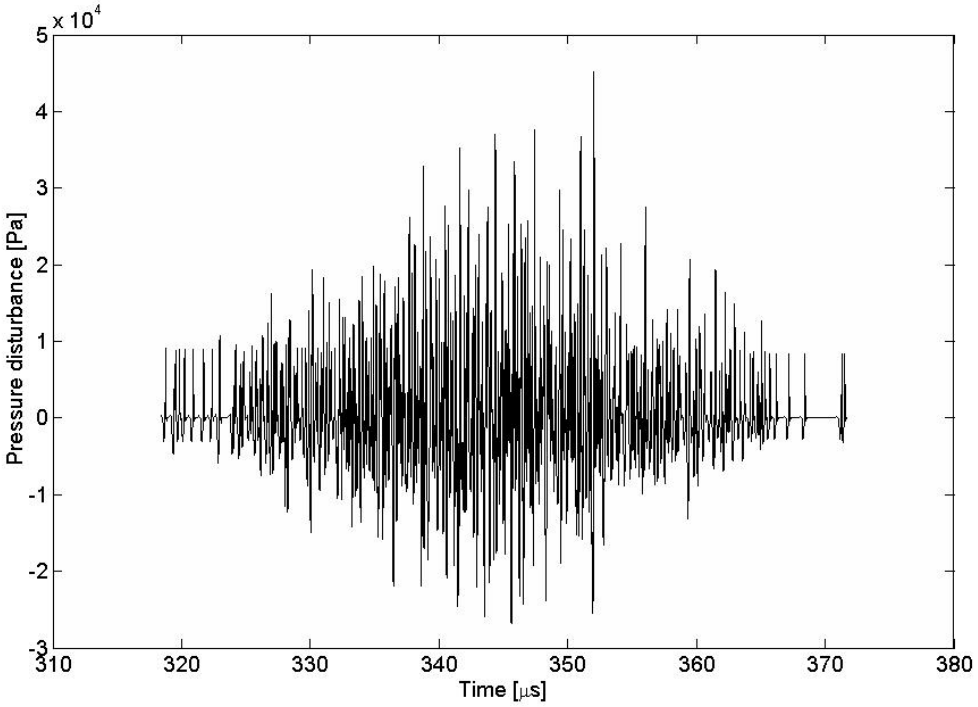

Fig.7 The predicted pressure time history of a 'first burst' (compare with signal measured in Figure 2), 500 mm from focus centre, where 1000 bubbles are modelled as cavitating within the lithotripter focus [29]

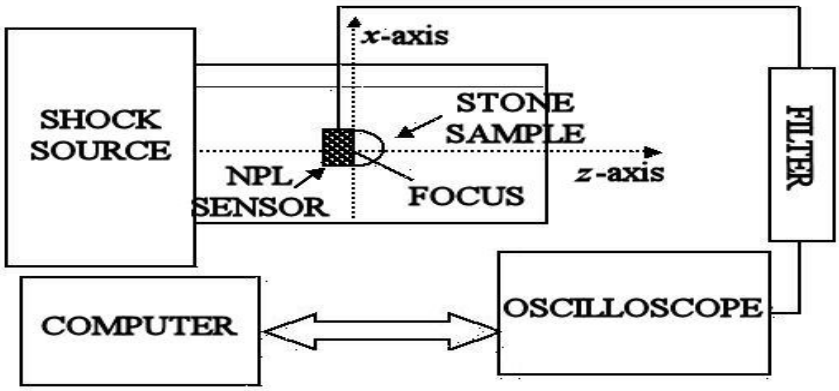

Fig.8 Schematic representation of the experimental set-up

3. LABORATORY STUDIES OF LITHOTRIPSY

In parallel to the CFD studies described in the previous section, an investigation on the possible exploitation of non focused passive sensors as diagnostic tools in lithotripsy started in January 2002. In particular, a novel cylindrical broadband sensor (up to 10 MHz) developed by the National Physical Laboratory (for monitoring cavitation in industrial applications [34, 35]) was tested in a laboratory facility at Guy's and St Thomas' NHS Foundation Trust. Figure 8

shows the experimental set-up; shockwaves were generated by means of an electromagnetic lithotripter operated under a voltage of 16kV to produce (at the focus) waveforms at pressures comparable to those expected *in vivo* (peak positive pressure P^+= 19±4 MPa, peak negative pressure P^-= 3±0.6 MPa). A high pass filter with a cut-off frequency of 200 kHz was used to remove background noise. The waveforms were recorded by means of a LeCroy 9354L digital scope operating at 100 MHz and then analysed off-line using MATLAB™. The analysis was aimed to identify important features in both the temporal history of the secondary emissions and the corresponding distribution of acoustic power over the frequency range of 0-2.5 MHz (which was considered to be clinically relevant). The digital signals were decimated at 5 MHz before performing any frequency processing. The details of the processing have been described in other publications [19-24, 36].

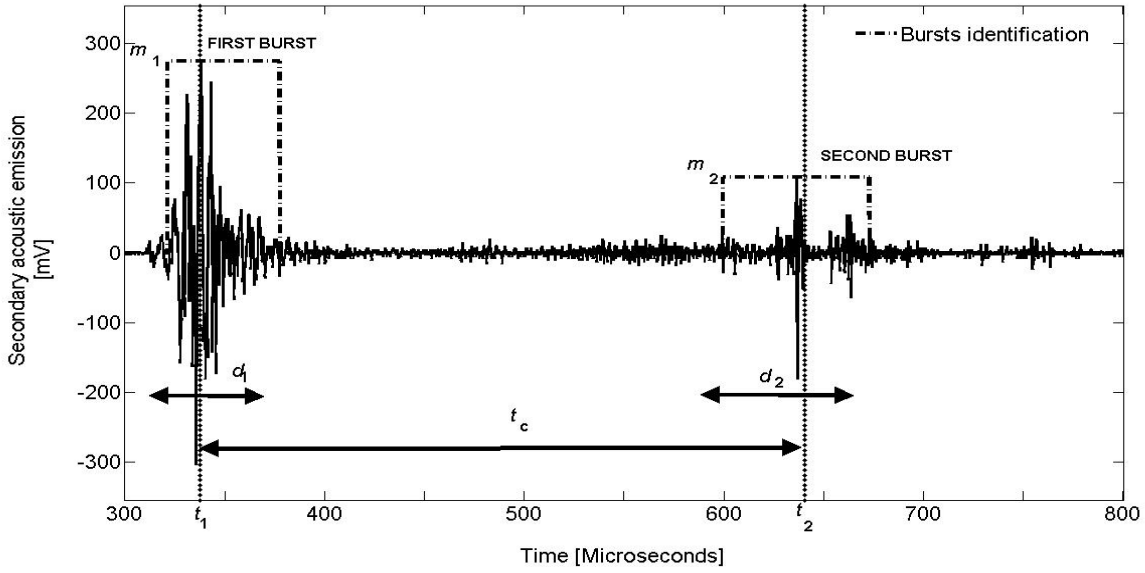

Fig.9 Example of the time domain analysis of an *in vitro* signal. The dash-dotted boxes delineate those two portions of the signals that are attributed two the first and second burst. The two bursts are separated by a collapse time t_c estimated as the interval between the two central times of the bursts (t_1 and t_2). Each of these bursts is then characterised in terms of a maximum amplitude (m_1 and m_2 respectively), and a duration (d_1 and d_2 respectively) [7, 19-24]. The kurtosis and skewness [37] of each of the two bursts (not reported in the figure) were also calculated [7, 24]

Figure 9 and Figure 10 report the main emissions features for a signal collected in tap-water. In particular, Figure 10 shows how the different mechanisms that contribute to the emission (mainly scattering for the first, and cavitation for the second) are reflected in different frequency distributions. The first burst contains most of its acoustic energy below 400 kHz, whilst the energy of the second burst is mainly distributed above 400 kHz [19-24, 36]. In order to quantify the power contributions in those two bands, for the two bursts, a Low Frequencies ratio (*LF*) and a High Frequencies ratio (*HF*) were defined as:

$$LF = \frac{\int_0^{f_{HI}} S_{qq}(f)df}{\int_0^{f_{max}} S_{qq}(f)df} \quad (1)$$

$$HF = \frac{\int_{f_{HI}}^{f_{max}} S_{qq}(f)df}{\int_0^{f_{max}} S_{qq}(f)df} \quad (2)$$

where f_{HI} is equal to 400 kHz, and f_{max} is equal to 2.5 MHz; and where $S_{qq}(f)$ indicates the power spectrum of the portion of signal $q(t)$ of interest (that is, either the first or second burst). That is to say, four parameters were derived: the low frequency ratio of the first burst (LF_1), the high frequency ratio of the first burst (HF_1), the low frequency ratio of the second burst (LF_2) and the high frequency ratio of the second burst (HF_2). In the example reported in Figure 10, LF_1=52%, HF_1= 48%, LF_2= 26% and HF_2= 74%.

The study progressed to examine the influence of stone targeting and fragmentation on the features of the secondary emissions [36]. Three kinds of stone phantoms were used in the study: plaster stones [36], sieved stones and lime-glass phantoms [24]. The last two stone phantoms were used to simulate stones of same size, but at different stages of fragmentation [19-24, 36]. In particular, a fragmentation ratio F was defined for each glass phantom as the percentage decrease in weight from an ideal intact glass stone of the same dimensions [24]. In order to investigate the influence of targeting on the emissions, the variation of the main emissions parameters (m_1, m_2 and t_c) was examined when a cylindrical plaster of Paris stone phantom was moved around the lithotripter focus [19, 36]. Both the maximum amplitude of the first burst m_1 (linked to scattering from the targeting) and the collapse time t_c (associated with cavitation) were shown to be sensitive to targeting. In addition, the introduction of the stone on the acoustic field showed an increase in both features [19, 36]. Figure 11 reports the variations observed in the collapse time t_c. In particular, collapse times of 300 μs and higher are observed when the stone is on target.

Sieved stones and soda-lime glass phantoms were used to investigate the influence of fragmentation on the characteristics of the emissions. A preliminary time-frequency analysis of the emissions collected adjacent to sieved stone phantoms showed some increase in the contribute of the acoustic energy at high frequencies ($f > f_{HI}$) [19]. That is to say, the analysis showed a decrease in LF_1 and an increase in HF_2. However, when these experiments were repeated (with both sieved and glass phantoms) enough times to produce a statistically rigorous analysis which took into account the variability of these frequency parameters around the group average, the difference among different stone phantoms observed in these tests could not be considered to be statistically significant [22, 24]. Figure 12, for example, reports the variability showed by LF_1 and HF_2 for soda lime glass phantoms simulating stages of fragmentation ranging from 31% to 100% [24]. A similar behaviour showed the central frequencies of the two bursts (f_{01} and f_{02}).

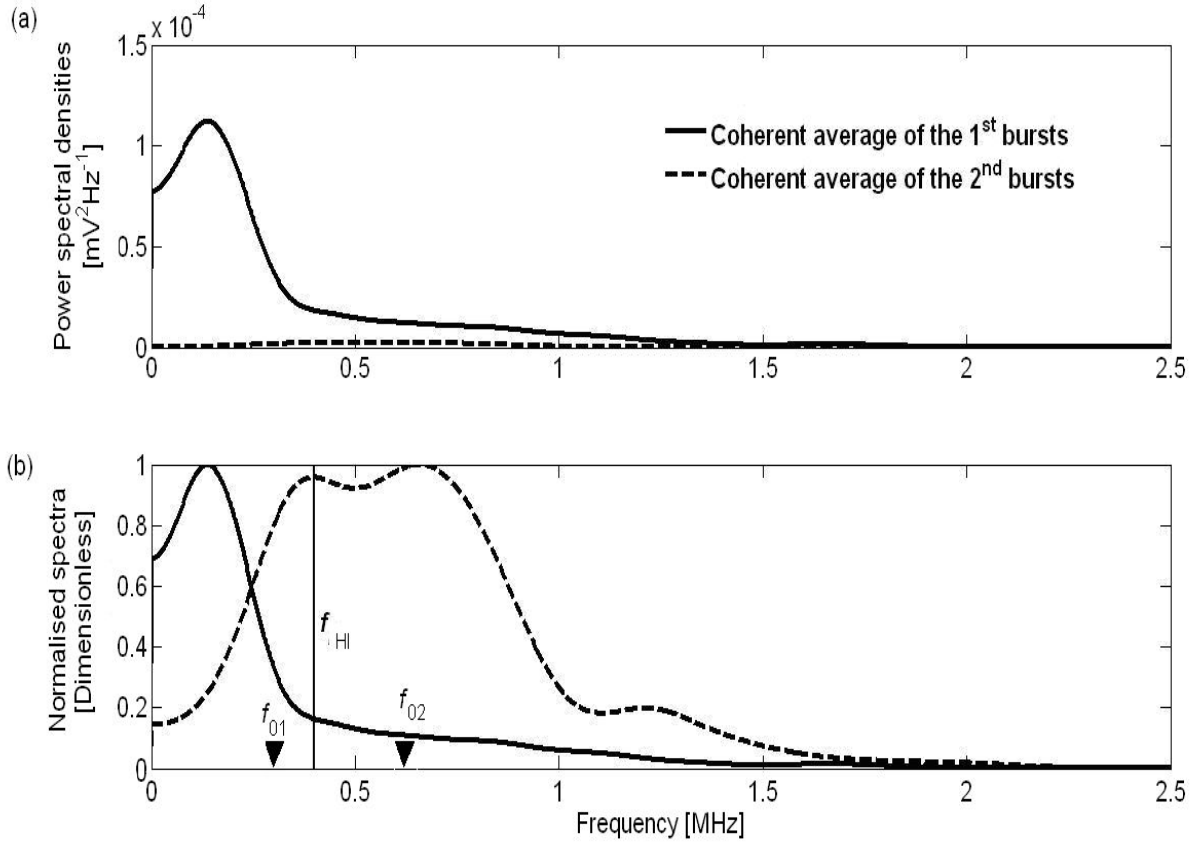

Fig.10 Example of the frequency domain analysis of an *in vitro* signal [7, 24]. Panel (a) shows the power spectral density (PSD) of the first burst (solid line) and the second burst (dotted line). The former contains a greater proportion of lower frequency energy ($< f_{HI} = 0.4$ MHz) because in addition to cavitation emissions, it contains the reflected energy of the incident lithotripter pulse (which the second burst lacks). To illustrate this more clearly, in panel (b) the two PSDs from the upper plot are normalised so that their maximum is unit (upper box). The central frequencies of the two bursts (f_{01} and f_{02} respectively) are also shown. In this case the frequency power ratios were LF_1=52%, HF_1= 48%, LF_2= 26%, HF_2= 74%

At this time in the study, a key decision had to be made on which parameters the clinical device should measure in order to provide real-time feedback in theatre of the effectiveness of each individual lithotripter shock. The variability seen in the study of the spectral characteristics, outlined above, suggested that all the frequency parameters considered here did not appear reliable predictors to use in real-time monitoring of clinical lithotripsy treatments (which would not have the benefit of acquiring large datasets for statistical analysis). They were consequently excluded from further analysis in favour of parameters which could be derived from the time history [22, 24]. It should however be noted that these conclusions refer only to the data taken in this study, in that a decision had to be made as to which method was proving to be most fruitful for the development of a successful clinical device. As such, the variability seen in our frequency measurements was indicating that, if a significant discrimination in the frequency characteristics were to be identified, it would in theatre take a large number of measurements, and therefore would not be practicable for the real-time shock-by-shock diagnostic system we were trying to

design. Other authors have since reported promising *in vitro* results from frequency analysis of the passive acoustic emissions of lithotripsy [38].

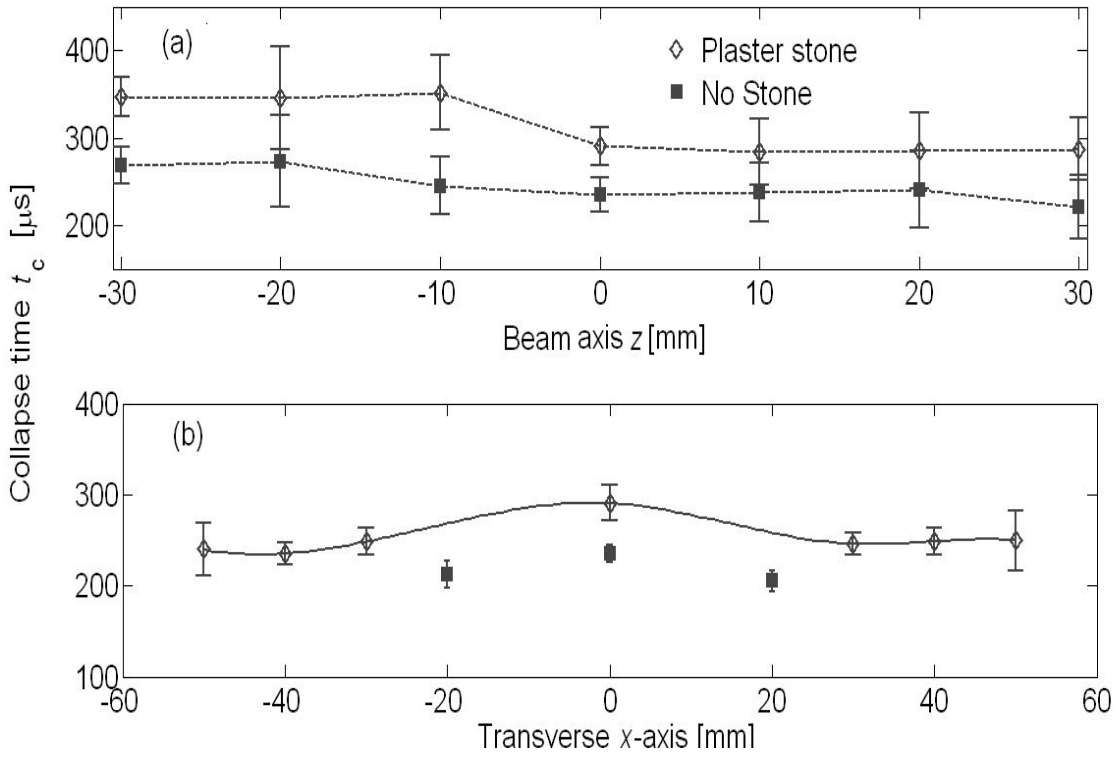

Fig.11 Variability in the collapse time t_c, when a plaster stone phantom is moved along (a) the beam axis and (b) off–axis of the bench-top lithotripter. The values (empty diamonds) are compared against reference values (solid squares) obtained moving the NPL sensor around the focus in absence of any stone sample. Each point is the average of five measurements and the error bars indicate ± one standard deviation from the average. The dotted lines in (a) indicate a linear interpolation. The solid line in (b) indicates a spline interpolation

On contrast, all the main features of the emissions extracted from the time history (m_1, m_2, t_c and the ratio of the two amplitudes m_2/m_1) were able to discriminate between different stages of fragmentation, with the potential for real-time application in theatre. For example, reference [24] reports the variability observed in the ratio m_2/m_1 (Figure 13). It can be noted that the stone phantoms with a considerable grade of fragmentation (F>50%) showed a ratio m_2/m_1>0.35.

On the basis of these preliminary *in vitro* experiments and the results of the CFD simulations (Section 2), a first clinical prototype passive sensor was developed in 2004 [19-24]. Three different passive prototypes were developed (Figure 14). The first prototype, referred to as Mark I (Figure 14(a)), was a square multi-channel sensor.

The three channels differed for a different diameter of the Polyvinylidene Fluoride (PVdF) sensitive element. That is to say, channel 1 was connected to a 1 mm sensitive element, channel 2 was connected to a 2 mm sensitive element and channel 3 was connected to a 3 mm element. The

four features (m_1, m_2, m_2/m_1 and t_c) of the emissions extracted from the three channels did not appear significantly different when this prototype was tested *in vitro*. In addition, when tested *in vivo*, the channel at the highest sensitivity (channel 3) showed a poor signal to noise ratio. In fact, this ratio was less than 50% also for patients with regular body mass index (BMI<25). In addition, patients showed a certain dislike and diffidence towards the appearance of this prototype. This is because they are used to the application of either round or flat sensors (i.e. ECG leads) or anyway sensors with smooth rounded surfaces (i.e. ultrasound probes). Such was the dislike of this prototype that the rate of acceptance to participate in the trial was low (about 30%). Therefore, for both technical and aesthetical reasons, such multi-channel design was abandoned to move towards a round smooth single channel sensor that could make the patient feel comfortable. The second prototype (Mark II), not reported in Figure 14, had the same appearance of the latest (Mark III, Figure 14(b)). Both Mark II and Mark III have a larger sensitive element than those used in Mark I. This element is 18 mm in diameter. The only difference in the two versions is the external diameter (20 mm vs. 25 mm), as Mark II had a smaller layer of protecting backing material than Mark III. The signals collected *in vitro* with all the prototypes showed similar characteristics to those collected with the NPL sensor [19, 20, 24]. It was *in viv*o that the three prototype showed different performances (see Section 4).

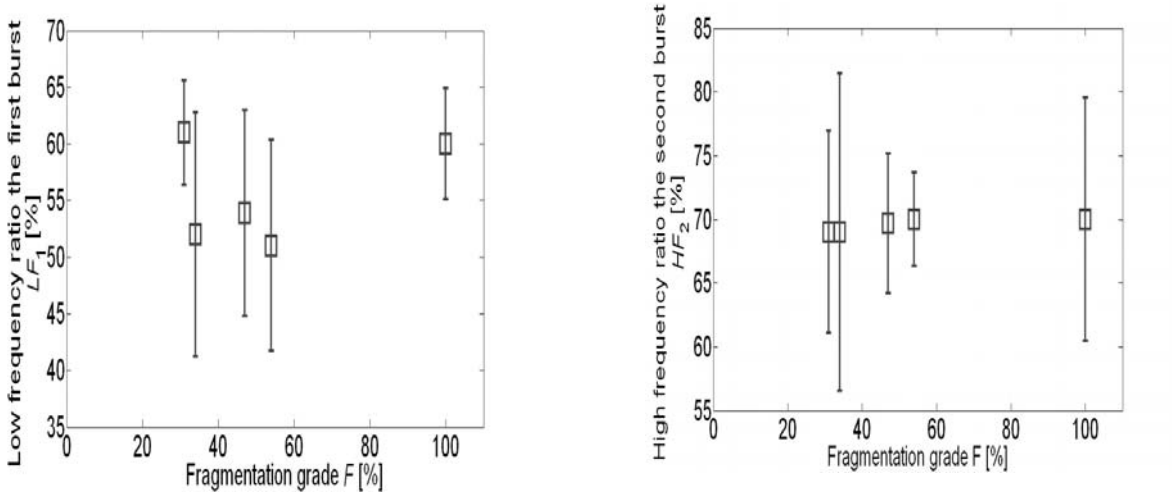

Fig.12 (a) Low frequency ratio of the first burst LF_1 and (b) high frequency ratio of the second burst HF_2 for soda-lime stone phantoms at different grades of fragmentation. The average value over 10 measurements is shown for each set and the error bars represent ± one standard deviation from the average of each set [24]

4. INITIAL IN VIVO STUDIES

As described in section 1, in 1992 Coleman, Leighton and co-workers [11] proved the presence of cavitation during ESWL and were able to monitor it *in vivo* by the recording of the associated secondary acoustic emissions. This was achieved by placing a passive acoustic sensor (the focused bowl of Figure 3) on the patient's abdomen. It was also shown that cavitation was generated within regions of increased echogenicity in the ultrasound image. In the late 1990s, as

explained in section 1, secondary acoustic emissions were recorded during clinical treatments (exploiting the same focused sensor) and analysed in the time frequency domain [25]. Then (as detailed in the previous section) the study progressed with the development of a first unfocused prototype system [19-24], that was tested *in vivo* for the first time in August 2003. This trial (aimed at testing and refining the system) lasted till October 2004 and involved 51 patients [24]. The result of the trial was the development of the data acquisition module of the PAS system, from one using only an early multichannel prototype sensor (the Mark I, shown in Figure 14(a)) to the final module that uses a single channel prototype sensor (the Mark III, shown in Figure 14(b)) in conjunction with a commercial preamplifier (HP1, Precision Acoustics, Dorchester, UK) and a high pass filter with a cut-off frequency of 292 kHz at 3 dB (custom-made for the project by Precision Acoustics, Dorchester, UK). Each component was tested for electrical safety before its use *in vivo* and the trial received the approval of Guy's and St. Thomas' NHS Trust Ethic Committee (Reference 06/Q0702/12). In compliance with the rules of this committee, consent was obtained before enrolling any patient in the trial. The final data acquisition module provided data of good quality (signal to noise ratio greater than 50%) for all 6 patients (among the 51) on whom it was tested. This stage was also used to analyse the features of the acoustic emissions *in vivo* and to compare them against treatment outcomes. The treatment outcomes were established by the urologist at the patient follow-up examination 2-3 weeks after the treatment. The results of this comparison helped the development of the signal processing module of the diagnostic system, and in particular they were exploited to develop an interface to synchronise the operations of data acquisition with the following processing to perform on-line monitoring [24]. This information was then used in the design of the clinical studies proper, which are described in the next section.

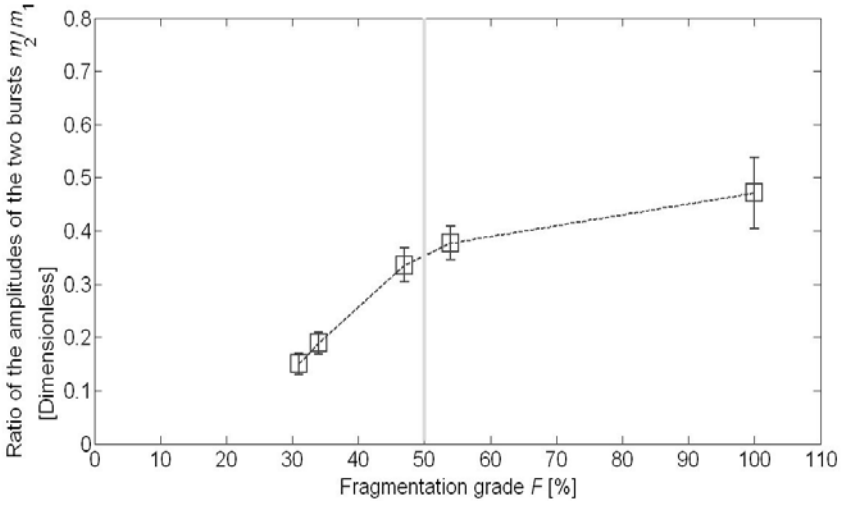

Fig.13 Ratio of the maximum amplitudes of the two burst m_2/m_1 for soda-lime stone phantoms at different grades of fragmentation. The average value over 10 measurements is shown for each set and the error represent ± one standard deviation from the average of each set. The dotted line indicates the linear interpolation between the average points [24]

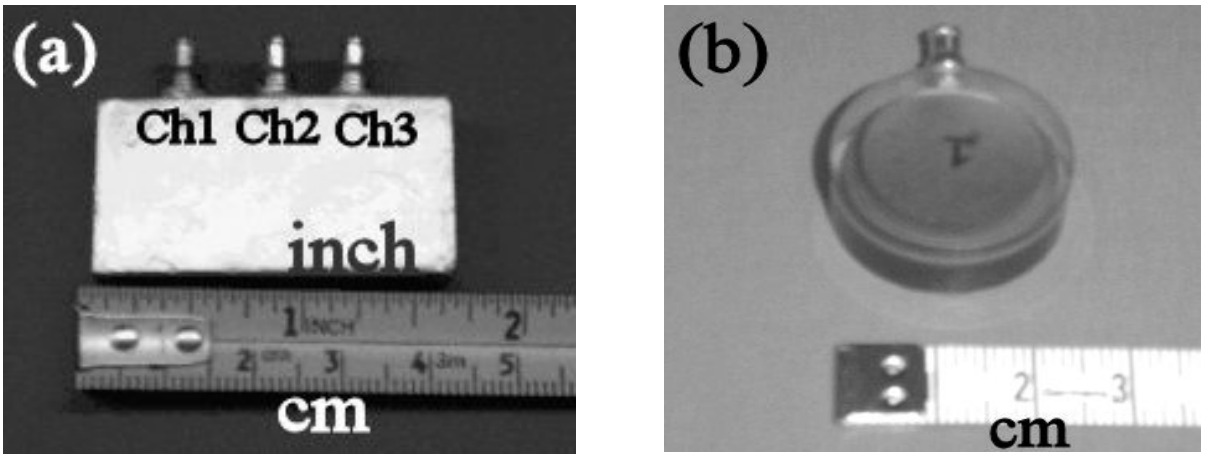

Fig.14 (a) First clinical prototype passive multi-channel ultrasound sensor, referred to as Mark I. (b) Final clinical passive ultrasound prototype sensor, referred to as Mark III

5. CLINICAL TRIALS

Having completed the initial *in vivo* studies (described in the preceding section), the research moved onto two clinical studies. These clinical trials are reported in detail in Leighton *et al.* [7] and only a brief overview will be given here. The studies of Sections 3 and 4 had confirmed that characterization of each echo in terms of the ratio m_2 / m_1 and the interval between the 'bursts' would be worth investigating to assess to what extent they could be used to judge the effectiveness of each shock in contributing towards the required end product (i.e. sufficient stone fragmentation). Specifically (noting that the precise method for working out the interval between bursts was amended slightly to make it more robust [7]) the *in vitro* tests indicated that a possible criterion for determining if a shock had been 'effective' in targeting and fragmenting the stone could be based on the requirement that $m_2 / m_1 > 0.4$ and $t_c \sim 300$ μs [24]. Phase 1 of the clinical studies described in this paper has examined validity and application of these 'rules' to the *in vivo* tests, and found that in the clinical situation the precise values needed amending. In phase 1, a complete set of acoustic and clinical data was obtained in 30 of the 118 subjects recruited. It was decided, on the basis of the clinical data from phase 1, to alter the *in vitro* 'rules' such that an 'effective' shock is defined as one in which both $0.40 < m_2 / m_1 < 0.8$ and $t_c > 100$ μs. These rules define a region shown as a box in Figures 15(a) and 15(b). The 'successful' treatments (as judged by the CTS_2; see Leighton *et al.* [7] for details) tend to generate echoes which cluster in these boxes [7] .

These clinically derived rules were then applied in a second clinical study in which complete data sets were obtained in 49 of the 85 subjects recruited. This second clinical study (Phase 2) demonstrated almost perfect agreement (kappa=0.94) between the number of 'successful' treatments, defined as greater than 50% fragmentation as determined by X-ray at the follow-up appointment, and a device-derived global treatment score, TS_0, a figure derived from the total number of 'effective' shocks in any treatment. The acoustic system is shown to provide a test of the 'success' of the treatment that has a sensitivity of 91.7% and a specificity of 100%. In addition to the predictive capability, the device provides valuable real-time feedback to the

lithotripter operator by indicating the effectiveness of each shock, plus an indication $TS(t)$ of the cumulative effectiveness of the shocks given so far in any treatment, and trends in key parameters. This feedback would allow targeting adjustments to be made during treatment. An example is given of its application to mis-targeting due to respiration. Details are provided in Leighton *et al.* [7].

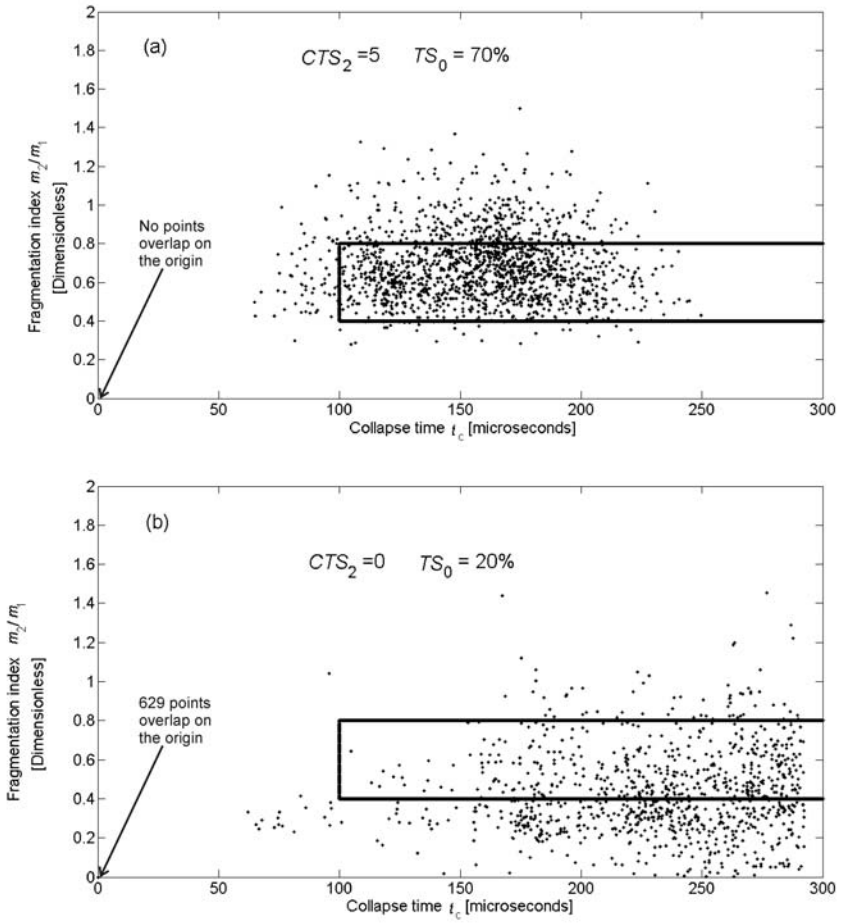

Fig.15 Plots from phase 1 of the clinical study giving the values of the acoustic parameters m_2 / m_1 and t_c for each shock from two sample treatments. The first plot (a) is for a 'successful' treatment as classified by the clinician from the X-rays (CTS_2 =5);the second plot (b) is for an 'unsuccessful' treatment as classified by the clinician from the X-rays (CTS_2 =0); see Leighton *et al*. for an explanation of the CTS_2 score. The area delimited by the solid line ($0.4< m_2 / m_1 <0.8$ and $t_c >100$ μs) represents the semi-empirical rules that appear from the phase 1 study to give the optimum indication of 'effective' and 'ineffective' shocks. It is postulated from the phase 1 study that a large number of 'effective' shocks (i.e. falling within the solid lines) result in a 'successful' treatment. Note that whilst Figure 9(a) contains no points at the origin, Figure 9(b) contains 629 overlapping points at the origin (see Leighton *et al.* [7] for details)

6. CONCLUSIONS

This paper describes the sequence of studies which led to the first passive acoustic detector for the efficacy of extracorporeal shock wave lithotripsy treatment which has been proven in clinical trials. Whilst the scope of the ethical approval did not allow the output of the sensor to be communicated in theatre to the clinicians (which therefore prevented our testing whether use of the device affects retreatment rates), the study has indicated the clinical usefulness of this technology.

Fig.16 Copy of the web page of NHS London Innovations showing AC, FF and TGL at the awards dinner on 26 November 2007

ACKNOWLEDGEMNTS

The Engineering and Physical Sciences Research Council provided a grant from 2000 to 2003 (EPSRC grant, GR/N19243/01, Principle Investigator: TG Leighton; Co-Investigator: AJ Coleman), which was followed by a further grant from 2005 to 2006 (Grant ref: EP/D503310/1; Principle Investigator: TG Leighton; Co-Investigator: AJ Coleman). However over this seventeen-year project, much of the work was undertaken without sponsorship (the average annual income to cover all costs was less than £20k). As such the project relied heavily on the generous donation of equipment and service in kind from a range of munificent sources. From the partner company Precision Acoustics Ltd., T. Gill and D. Bell provided invaluable assistance in developing the passive sensor. R. Tiptaft, J. Glass, D. Phillips and T. Jessop (Urology Department at Guy's and St Thomas' NHS Trust) are gratefully acknowledged for their support during the clinical study. From the UK National Physical Laboratory, B. Zeqiri, M. Hodnett and

and C. Bickley were unstinting in their loans of their cavitation detectors for cross-comparison with the sensors used *in vitro* in the laboratory stages of this research reported in Section 3. C. McKinnon (Centre for Enterprise and Innovation, University of Southampton) and T. Parlett (Intellectual Property Officer, Guy's & St Thomas' NHS Trust) are thanked for their work in the contractual and commercial aspects of this study. From ISVR, D. Finfer is thanked for assistance in software programming, G. T. Yim is thanked for his advice on computing hardware, and V. Humphrey is thanked for loan of interim replacement transducers and preamplifiers when the apparatus was sent for servicing. NHS Innovations London were kind enough to shortlist the device for their award in 2008 (Figure 16). All clinical work was approved by the local research ethics committee of Guy's and St Thomas' NHS Foundation Trust.

REFERENCES

1. C. Chaussy and E. Schmiedt, " Shock wave treatment for stones in the upper urinary tract," *J. Urol. Clin. North Am. ,* vol. 10, pp. 743-750, 1983.
2. Y. M. Tan, S. K. Yip, T. W. Chong, M. Y. Wong, C. Cheng, and K. T. Foo, "Clinical experience and results of ESWL treatment of 3,093 urinary calculi with the Storz Modulith SL 20 lithotripter at the Singapore general hospital," *Scand. J. Urol. Nephrol.,* vol. 36, pp. 363-367, 2002.
3. B. Auge and G. Preminger, "Update on shockwave lithotripsy technology," *Curr. Opin. Urol.,* vol. 12, pp. 287-290, 2002.
4. J. E. Lingeman, D. M. Newman, H. H. O. Mertz, Ph. G. Mosbaugh, R. E. Steele, P. M. Knapp, and W. Shirell, "Management of upper ureteral calculi with ESWL," in IV World Congress on Endurology and ESWL Madrid 1986.
5. D. Tolley and P. Downey, "Current advances in shock wave lithotripsy," *Curr. Opin. Urol.,* vol. 9, pp. 319-323, 1999.
6. A. Skolarikos, G. Alivizaos, and J. de la Rosette, "Extracorporeal shock wave lithotripsy 25 years later: complications and their prevention," *Eur. Urol. ,* vol. 50, pp. 981-990, 2006.
7. T. G. Leighton, F. Fedele, A. J. Coleman, S. Ryves, C. McCarthy, A. M. Hurrell, A. D. Stefano, and P. R. White, "A device for monitoring the efficacy of ESWL using passive acoustic emissions, Ultrasound in Medicine and Biology," *Ultrasound in Medicine and Biology (in press),* 2008
8. D. Delakas, I. Karyotis, G. Daskalopoulos, E. Lianos, and E. Mavromanolakis, "Independent predictors of failure of shockwave lithotripsy for ureteral stones employing a second-generation lithotripter," *J. Endourol.,* vol. 17, pp. 201-205, 2003.
9. M. A. Gomha, K. Z. Sheir, S. Showky, M. Abdel-Khalek, A. A. Mokhtar, and K. Madbouly, "Can we improve the prediction of stone-free status after extracorporeal shock wave lithotripsy for ureteral stones? A neural network or statistical model?," *J. Urol. ,* vol. 172, pp. 175-179, 2004.
10. M. A. Warner, M. E. Warner, C. F. Buck, and J. W. Segura, "Clinical efficacy of high frequency jet ventilation during extracorporeal shock wave lithotripsy of renal and ureteral calculi: a comparison with conventional mechanical ventilation," *J. Urol.,* vol. 139, pp. 486-487, 1988.

11. A. J. Coleman, M. J. Choi, J. E. Saunders, and T. G. Leighton, "Acoustic emission and sonoluminescence due to cavitation at the beam focus of an electrohydraulic shock wave lithotripter," *Ultrasound in Medicine and Biology,* vol. 18, pp. 267-81, 1992.
12. S. Madaan and A. D. Joyce, "Limitations of extracorporeal shock wave lithotripsy," *Curr. Opin. Urol. ,* vol. 17, pp. 109-113, 2007.
13. R. M. Schmitt, H. Wuster, W. Kraus, and M. Bibinger, "The effects of errors in positioning lithotripter and imaging kidney stones ultrasound," in *Proceedings of the Annual international conference of the IEEE Engineering in Medicine and Biology Society* 1990, pp. 252-253.
14. P. Sandilos, I. Tsalafoutas, G. Koutsokalis, P. Karaiskos, E. Georgiou, E. Yakoumakis, and L. Vlahos, "Radiation doses to patients from extracorporeal shock wave lithotripsy " *Health Phys.,* vol. 90, pp. 583-587, 2006.
15. A. J. Coleman, M. Whitlock, T. G. Leighton, and J. E. Saunders, "Spatial distribution of cavitation induced acoustic emission, sonoluminescence and cell lysis in the field of a shock wave lithotripter," *Physics in Medicine and Biology,* vol. 38, pp. 1545, 1993.
16. T. G. Leighton, *The Acoustic Bubble*. London: Academic Press, 1994.
17. T. G. Leighton, "From seas to surgeries, from babbling brooks to baby scans: the acoustics of gas bubbles in liquids," *International Journal of Modern Physics B,* vol. 18, pp. 3267-314, 2004.
18. C. K. Turangan, A. R. Jamaluddin, G. J. Ball, and T. G. Leighton, "Free-Lagrange simulations of the expansion and jetting collapse of air bubbles in water," *Journal of Fluid Mechanics,* vol. 598, pp. 1-25, 2008.
19. T. G. Leighton, A. J. Coleman, F. Fedele, and P. R. White, "A passive acoustic system for evaluating the in-vivo performance of extracorporeal shockwave lithotripsy." UK Patent Num. 0319863.7, 2004.
20. F. Fedele, A. J. Coleman, T. G. Leighton, P. R. White, and A. M. Hurrell, "A new sensor for detecting & characterising acoustic cavitation in vivo during ESWL," in *Proceedings of the Institute of Acoustics*. vol. 26(1), 2004, pp. 422-432.
21. F. Fedele, A. J. Coleman, T. G. Leighton, P. R. White, and A. M. Hurrell, "A new sensor for detecting and characterising acoustic cavitation in vivo during ESWL," *Acoustics Bulletin,* vol. 29, pp. 34-39, 2004.
22. F. Fedele, A. J. Coleman, T. G. Leighton, P. R. White, and A. M. Hurrell, "Development of a new diagnostic device for Extracorporeal Shock-Wave Lithotripsy," in *Proceedings of the X Mediterranean Conference on Medical and Biological Engineering "Health in the Information Society" (IFMBE Proceedings volume)*. vol. 6, paper no. 54, 2004 (4 pages).
23. F. Fedele, A. J. Coleman, T. G. Leighton, P. R. White, and A. M. Hurrell, "Development of a new diagnostic sensor for extracorporeal shock-wave lithotripsy," *Journal of Physics: Conference Series,* vol. 2, pp. 125-30, 2004.
24. F. Fedele, "Acoustic sensing of renal stones fragmentation in extracorporeal shockwave lithotripsy," in *PhD thesis, University of Southampton*: Southampton, 2008 (submitted).
25. K. B. Cunningham, A. J. Coleman, T. G. Leighton, and P. R. White, "Characterising in vivo acoustic cavitation during lithotripsy with time-frequency methods," *Acoustics Bulletin,* vol. 26, pp. 10-16, 2001.
26. T. G. Leighton, B. T. Cox, and A. D. Phelps, "The Rayleigh-like collapse of a conical bubble," *Journal of the Acoustical Society of America,* vol. 107, pp. 130-142, 2000.

27. T. G. Leighton, W. L. Ho, and R. Flaxman, "Sonoluminescence from the unstable collapse of a conical bubble," *Ultrasonics,* vol. 35, pp. 399-405, 1997.
28. T. G. Leighton, B. T. Cox, P. R. Birkin, and T. Bayliss, "The Rayleigh-like collapse of a conical bubble: Measurements of meniscus, liquid pressure, and electrochemistry," in *Proceedings of the 137th Regular Meeting of the Acoustical Society of America and the 2nd Convention of the European Acoustics Association (Forum Acusticum 99, integrating the 25th German Acoustics DAGA Conference)*, 1999, Paper 3APAB_1.
29. A. R. Jamaluddin, "Free-Lagrange simulations of shock–bubble interaction in ESWL." PhD: University of Southampton, 2006.
30. G. J. Ball, B. P. Howell, T. G. Leighton, and M. J. Schofield, "Shock-induced collapse of a cylindrical air cavity in water: a Free-Lagrange simulation," *Shock Waves,* vol. 10, pp. 265-76, 2000.
31. G. J. Ball, B. P. Howell, T. G. Leighton, and M. J. Schofield, "Shock-induced collapse of a cylindrical air cavity in water: a Free-Lagrange simulation," in *The 22nd International Symposium on Shock Waves* London, 2000, pp. 1363-1368.
32. A. R. Jamaluddin, G. J. Ball, and T. G. Leighton, "Free-Lagrange simulations of shock/bubble interaction in shock wave lithotripsy," in *The 24th International Symposium on Shock Waves* Beijing, China, 2004, pp. 1211-1216.
33. A. R. Jamaluddin, G. J. Ball, and T. G. Leighton, "Free-Lagrange simulations of shock/bubble interaction in shock wave lithotripsy," in *Proceedings of the Second International Conference on Computational Fluid Dynamics, ICCFD, Sydney, Australia*, 2002, pp. 541-546.
34. T. G. Leighton, P. R. Birkin, M. Hodnett, B. Zeqiri, J. F. Power, G. J. Price, T. Mason, M. Plattes, N. Dezhkunov, and A. J. Coleman, "Characterisation Of Measures Of Reference Acoustic Cavitation (COMORAC): An experimental feasibility trial," in *Bubble and Particle Dynamics in Acoustic Fields: Modern Trends and Applications*, A. A. Doinikov, Ed. Kerala: Research Signpost, 2005, pp. 37-94.
35. B. Zeqiri, P. N. Gelat, M. Hodnett, and N. D. Lee, "A novel sensor for monitoring acoustic cavitation. Part II: prototype performance evaluation," *IEEE Transaction on Ultrasonics, Ferroelectrics, and Frequency Control,* vol. 50, pp. 1351-1362, 2003.
36. F. Fedele, A. J. Coleman, and T. G. Leighton, "Use of a cylindrical PVdF hydrophone in a study of cavitation adjacent to stone phantoms during extracorporeal shockwave lithotripsy," in *Proc of the 9th Annual National Conference of the Institute of Physics and Engineering in Medicine* Bath, 2003, pp. 66.
37. A. Papoulis and S. U. Pillai, *Probability, Random Variables and Stochastic processes*. Singapore: McGraw-Hill., 2001.
38. N. R. Owen, M. R. Bailey, L. A. Crum, O. A. Sapozhnikov, and L. A. Trusov., "The use of resonant scattering to identify stone fracture in shock wave lithotripsy. ," *J Acoust Soc Am,* vol. 121, pp. EL41–EL46, 2007.